Single-Chip Micro Mote in EEG, fMRI, and TMS Systems

Joshua Alexander

Electrical Engineering and Computer Sciences
University of California, Berkeley

Technical Report No. UCB/EECS-2022-136
http://www2.eecs.berkeley.edu/Pubs/TechRpts/2022/EECS-2022-136.html

May 18, 2022

Single-Chip Micro Mote in EEG, fMRI, and TMS Systems

by Joshua Alexander

Research Project

Submitted to the Department of Electrical Engineering and Computer Sciences, University of California at Berkeley, in partial satisfaction of the requirements for the degree of **Master of Science, Plan II**.

Approval for the Report and Comprehensive Examination:

Committee:

Professor Kristofer Pister
Research Advisor

May 16, 2022

(Date)

* * * * * * *

Professor Chunlei Liu
Second Reader

Abstract

The goal of this project is to measure EEG signals in an MRI during TMS and report the EEG measurements wirelessly. The opportunities combining SoC-based devices with cutting-edge technology are rapidly expanding. A Single Chip Micro-Mote (SCμM) that has been developed as an ultra-small crystal-free SoC opens up the door of possibilities even more. Similarly, brain stimulation and measurement has taken a leap forward as Transcranial Magnetic Stimulation (TMS), Electroencephelography (EEG), and functional Magnetic Resonance Imaging (fMRI) have grown in popularity. A structure that combines all three elements by evaluating the EEG and fMRI brain response to TMS pulses would provide invaluable research opportunities. In order to help facilitate EEG measurements in TMS and fMRI environments, there is a need to pass the data out of the electrodes to an external computer for instant analysis. SCμM's ability to function in a variety of settings and environments make it an ideal candidate as a component of a system that combines these three practices, TMS, EEG, and fMRI, into combined operation. We were able to verify that SCμM functions during a MRI scan while connected to a printed battery. We were also able to confirm that SCμM does not reset under TMS impulses delivered 1 inch away from SCμM at relative amplitudes of up to 97%. We were unable to test SCμM on a new development board with an EEG analog front end (ADS1299) in an MRI, but we were able to communicate with the ADS1299 via SPI with the Sulu SCμM development board's GPIO pins.

Chapter 1

Introduction

The goal of this project is to measure EEG signals in an MRI during TMS and report the EEG measurements wirelessly. A small, versatile SoC with a crystal-free radio and microprocessor such as the Single-Chip Micro Mote (SCμM) has a wide variety of possible applications as it permits the ability to have a tiny and cheap housing for the chip and reliable communication with external components. Together with a standards-based protocol stack and corresponding communication device, the use cases for SCμM are ever-growing. Some of SCμM's many potential applications range from autonomous robot actuators, as seen in figure 1.1, [3] and a wireless hydrogen sulfide gas sensor system [7] to swarm robotics systems and tracking invasive Asian hornets in Europe as they fly back to their nests [8]. The on-chip optical receiver can be used in conjunction with lighthouse localization beacons in order to identify the location of SCμM in a 3D space with millimeter level accuracy [18]. One such application for SCμM would be to transmit EEG signals in a combined EEG-TMS-fMRI system. Wires transmitting EEG data or supplying power are undesirable since the gradient and RF fields of a MRI scan could induce a current in those wires. The current in those wires presents a safety risk as they can heat up and cause injury to a patient if it contacts their skin. SCμM's small size and ability to clearly transmit over established standards such as IEEE 802.15.4 or Bluetooth Low Energy while inside a scanner makes it an ideal candidate for this system. This report details how the current SCμM 3C chip behaves when placed in these types of situations and how it can be used to deliver EEG signals to a computer for analysis.

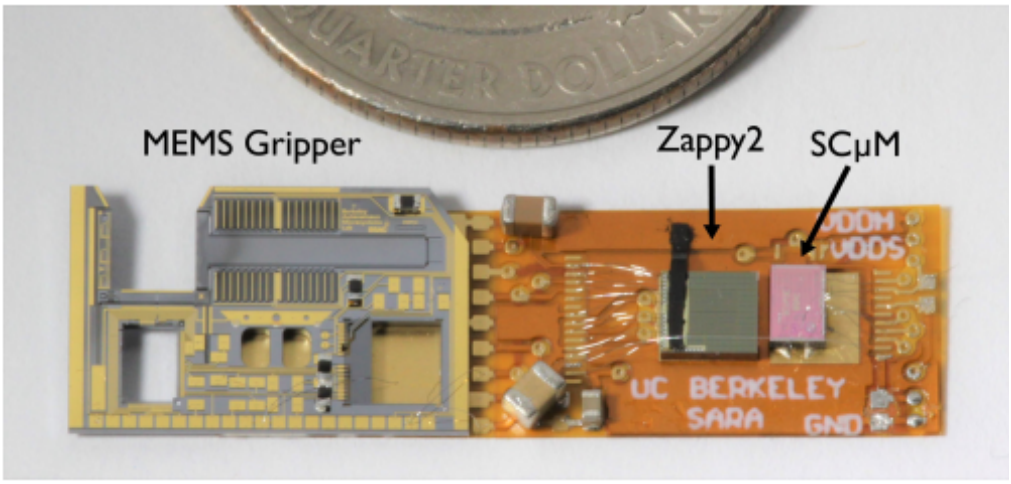

Figure 1.1: Small Autonomous Robot Actuator (SARA) [3]. Total area of 9.5x31.55mm^2

In a suggested EEG-TMS-fMRI configuration with SCμM detailed in figure 1.2, MRI scans and EEG readings would continuously provide information regarding a patient's neural activity. Meanwhile, a TMS coil will move around the patient's head, controlled via a robot to the following location desired for treatment based on the gathered measurements. This process will continue for multiple cycles until the treatment is deemed complete. SCμM does not need to transmit EEG data continuously throughout this process as artifacts from a TMS pulse could corrupt the readings, but it must be able to maintain its initial programming and resume transmission once the TMS phase of the current cycle of treatment has been completed. Table 1.1 outlines the current desired timing schedule. As such, SCμM must withstand TMS pulses and the large magnetic field in an MRI scanner to transmit data that captures minimal EEG signals during continuous MRI scanning.

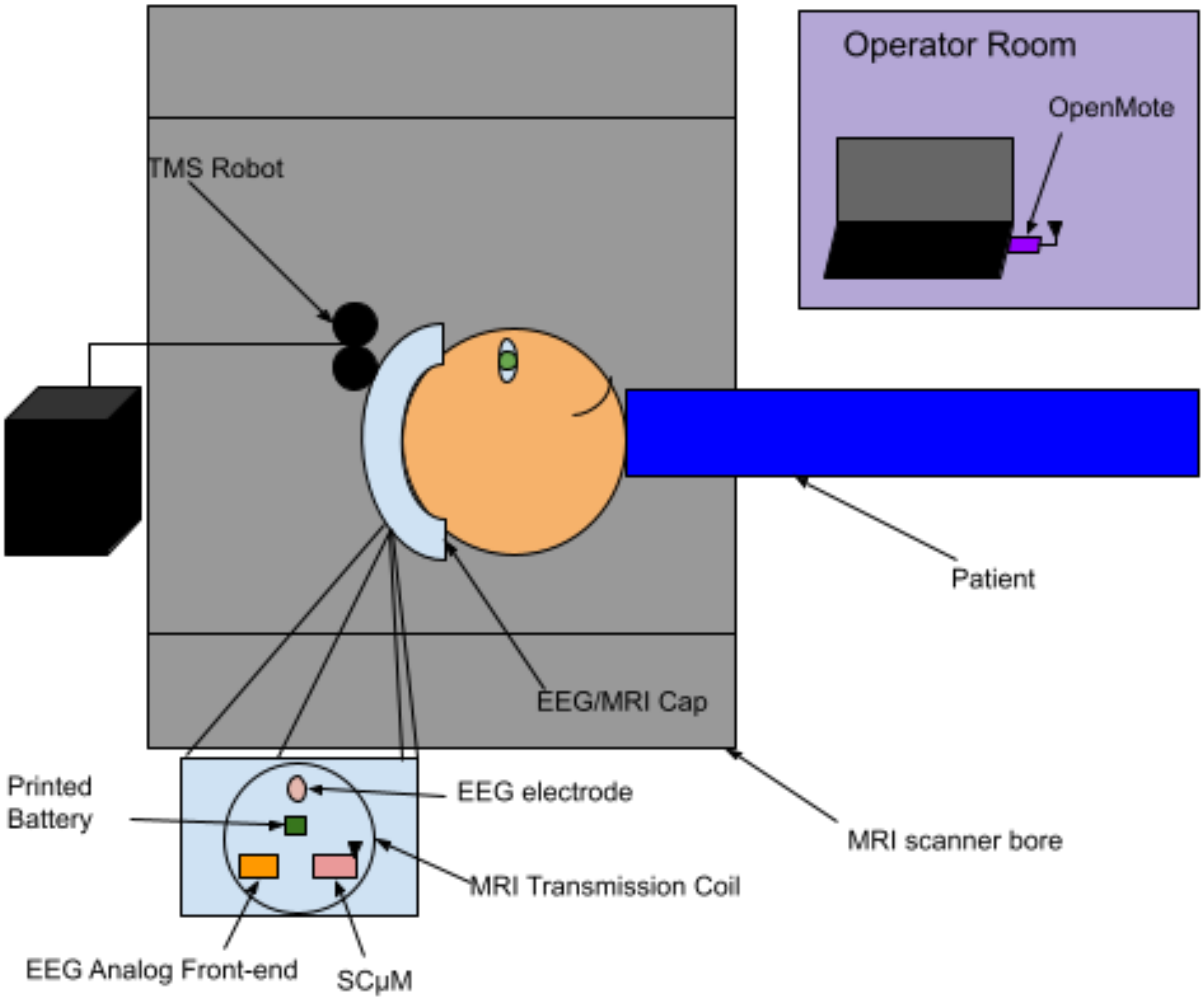

Figure 1.2: System diagram of TMS-EEG-fMRI final system

Cycle	Event Start Time (s)	Event End Time (s)	TMS Robot + Coil	EEG Interface	MRI	Signal Processing
1	0.000	3.530	Adjust the position of TMS robot	None	Idle	None
1	3.530	3.531	Passive hold position	Blank amps	Idle	None
1	3.531	3.541	10 ms biphasic pulse	Blank amps	Idle	None
1	3.541	33.541	Passive hold position	Read EEGs	MRI scan	None
2	33.541	37.071	Adjust the position of TMS robot	None	Idle	Determine next TMS robot position based on EEG/MRI results

Table 1.1: Timing schedule for TMS-EEG-fMRI system.

Chapter 2

Background on SCμM, OpenWSN, OpenMote, and TMS/EEG/fMRI Systems

2.1 SCμM

SCμM is a single-chip micro mote that is 2x3x0.3 mm with a built-in standards compatible IEEE 802.15.4 or BLE transceiver that can transmit below 1 mW peak power and a Cortex-M0 [1]. SCμM accomplishes this small size through crystal-free operation, a 65 nm CMOS process design, and an optical receiver that can be used for calibration or programming. The transceiver is able to function with only power, ground, and a bond wire antenna connected to SCμM [2]. As such, SCμM is a desirable option for use in a system that would combine EEG, fMRI, and TMS operation as its small required area of components to operate would allow an application that is able to transmit EEG signals wirelessly without interfering with the movement of the TMS coil and minimal wiring to be affected by an MRI scan. SCμM has 16 0.8V-3.6V GPIO pins which can be used to gather data from EEG signals to transmit [3] out of the system.

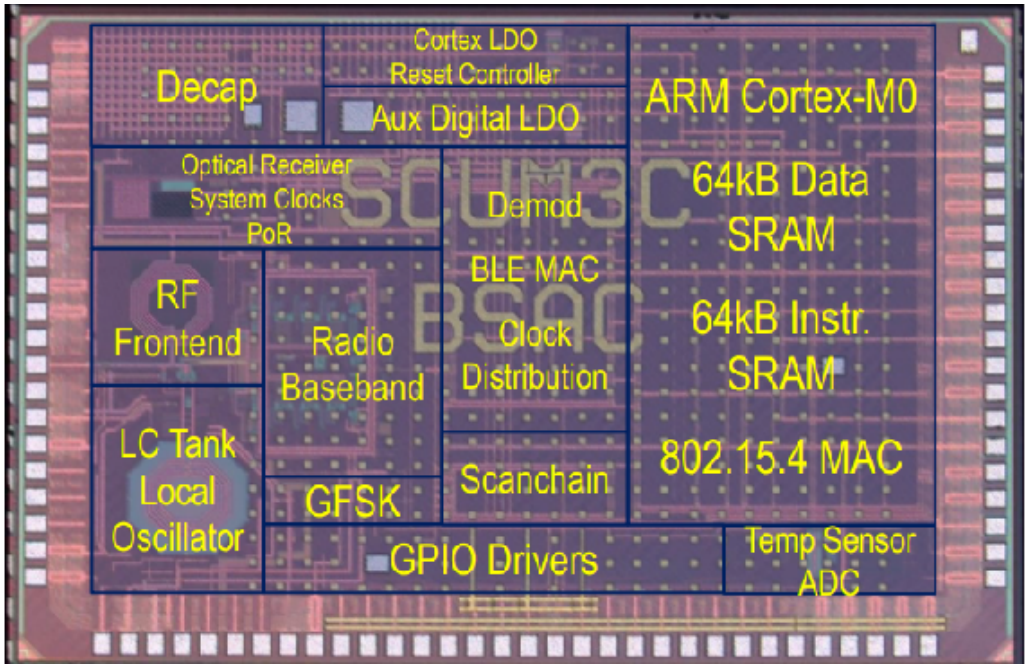

Figure 2.1: Single-Chip Micro Mote die photo [2]. Different regions of the chip have been labeled with what is contained within them. The dimensions of SCμM are 2x3x0.3mm^3

2.2 SCµM Development Boards

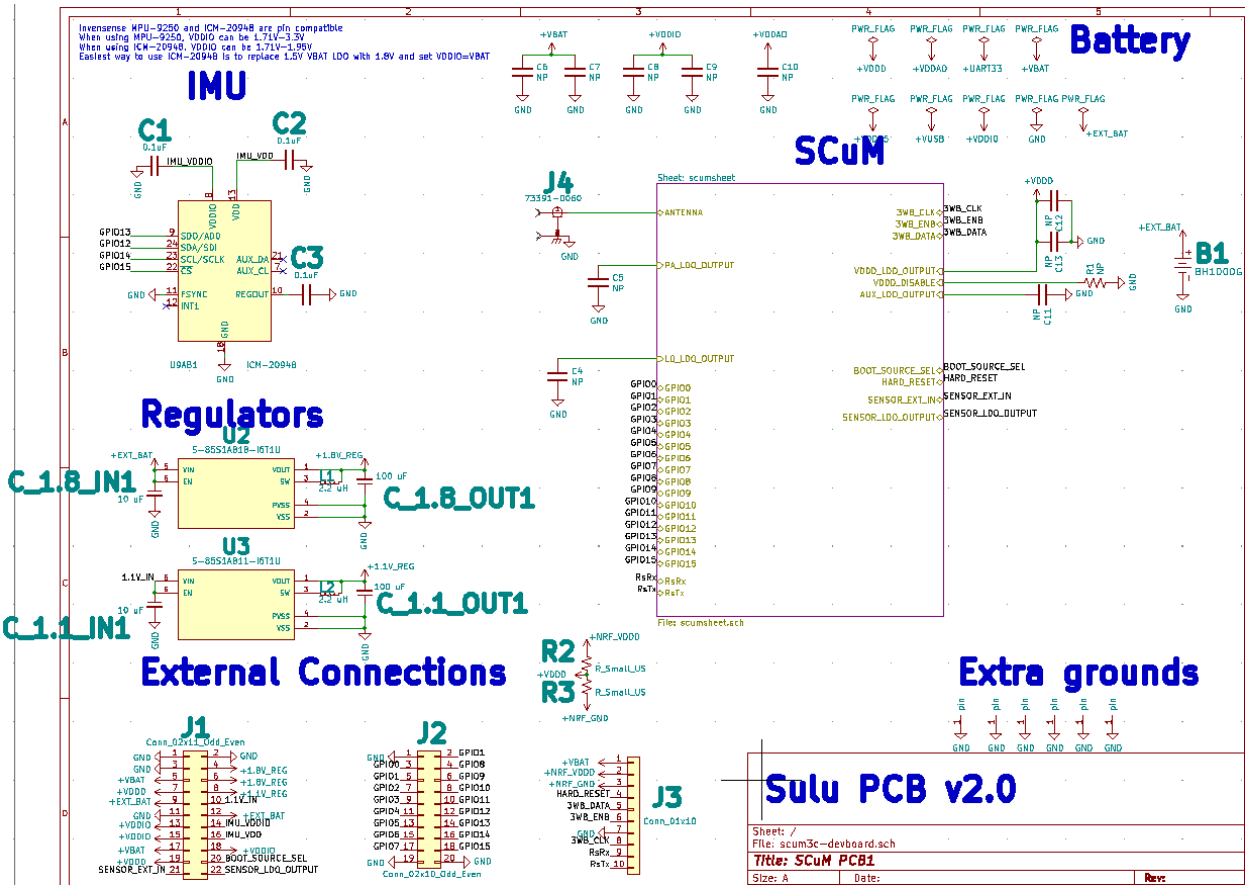

Figure 2.2: Sulu v2 development board schematic. Notable components are highlighted. The footprint for a coin cell battery holder is on the back of Sulu. All other components can be seen in figure 2.3. Capacitors next to SCµM are optional for decoupling purposes. R2 and R3 are for future use with an untested VDDD tap from an nRF52840-DK.

In order to ease the ability to test SCµM, a development board, Sulu, was created. It takes an input of about 5V and generates 1.8V for SCµM's VBAT and 1.1V for SCµM's VDDD via DC-DC step-down converters. Alternatively, SCµM's VBAT and VDDD inputs can be disconnected from the DC-DC step-down converters to be powered directly. For the purpose of the tests described below, an option with Low-Dropout regulators was also tested with no change in performance. For testing SCµM in the environments described, an SMA connector on Sulu was used in order to

easily attach an antenna to facilitate communication between SCμM and a receiver easily and more robustly confirm operation despite SCμM also being functional with a wirebonded antenna. SCμM itself is enclosed in an epoxy QFN package using QP Technologies' 60-7170 resin to protect the chip and wire bond connections.

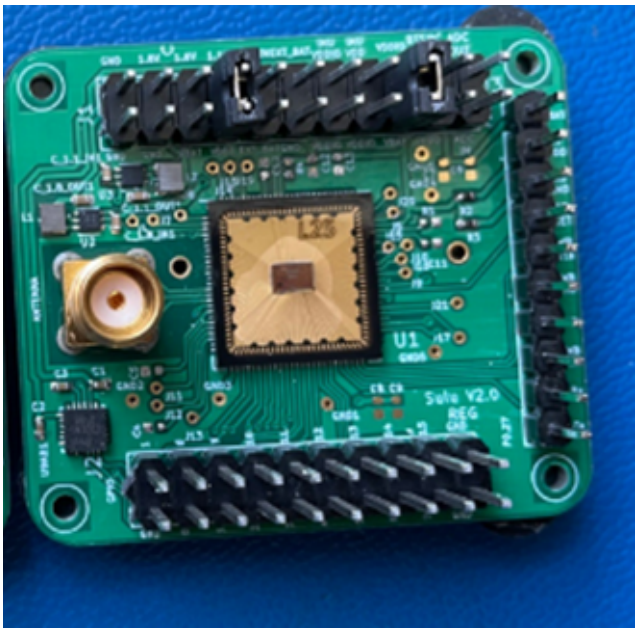

Figure 2.3: Fully assembled Sulu v2 development board. GPIO (bottom 2 rows of pin headers), power connections (top 2 rows of pin headers), and external communication connections (right row of pin headers)

SCμM can be programmed via two different methods toggled via the Boot Source Select input: optically using an optical bootloader or by using a 3 Wire Bus (3WB) connection to a device such as an nRF52840 DK. Data can be transmitted to and from the SCμM chip on Sulu via the UART Rx and Tx pin connections. A common configuration for testing SCμM powering and communicating the Sulu board with an nRF52840-DK can be seen in figure 2.4. With further testing using these development boards, special care must be taken to ensure the board traces and the packaged SCμM itself must be kept below 200° C so as not to damage the wirebond connections from SCμM. Use of a soldering iron to add any components is likely to damage the package as evidenced by melting or cracking the epoxy package sealant as seen in figure 2.5. Past success has been found

by attaching surface mount components with 150° C solder paste, then applying SMDLTLFPT5 Sn42/Bi57 no-clean solder paste to through-hole components and curing them on a covered hot plate.

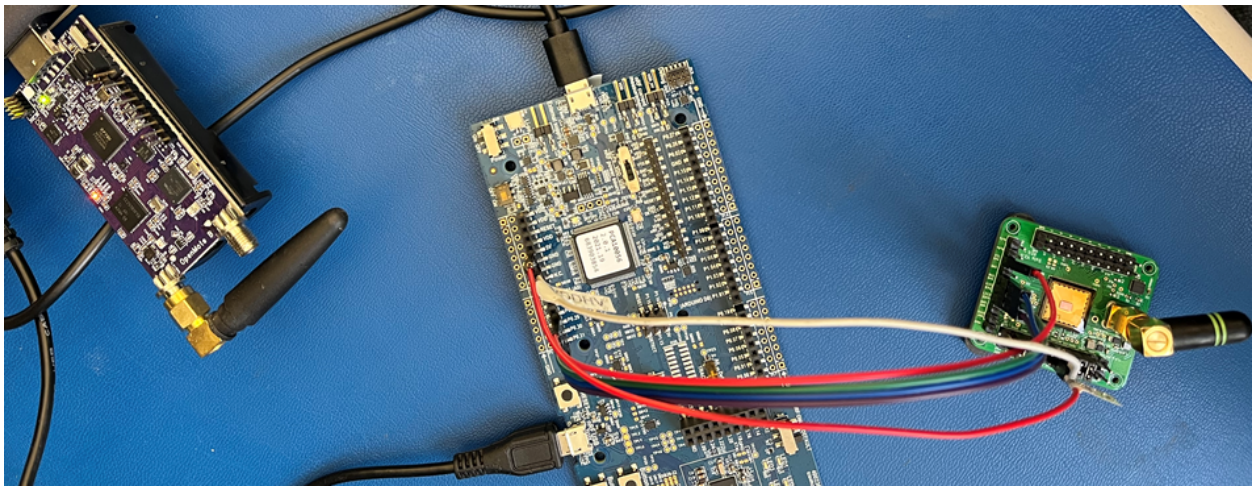

Figure 2.4: Sample setup for programming Sulu development board (right) via an nRF32840-DK (center) over 3WB and transmitting to an OpenMote B CC2538 (left)

Figure 2.5: Damaged packaged SCµM chip on Sulu due to adding through-hole components with a soldering iron. Connections to this SCµM chip have been irreparably damaged and Sulu is unable to get SCµM to boot.

2.3 Stencil-Printed Lithium-Ion Batteries

In order to supply power to Sulu, small, stencil-printed batteries were chosen. Stencil-printed lithium-ion batteries, pictured in figure 2.6, are designed with a graphite anode and a lithium cobalt oxide cathode accessed by copper and aluminum current collectors [13]. These printed batteries made an ideal candidate to incorporate with a 6.4 mAh/cm^2 capacity and verified compatibility with Sulu. While these batteries would be powering Sulu exclusively in a complete EEG-TMS-fMRI system, they can also be temporarily used to power off-chip components during the evaluation of SCμM's performance in this project's scenarios. They can be accessed via alligator clips or by attaching wires to the collectors using silver epoxy that cures at room temperature, as elevated temperatures can cause deterioration in battery functionality and capacity.

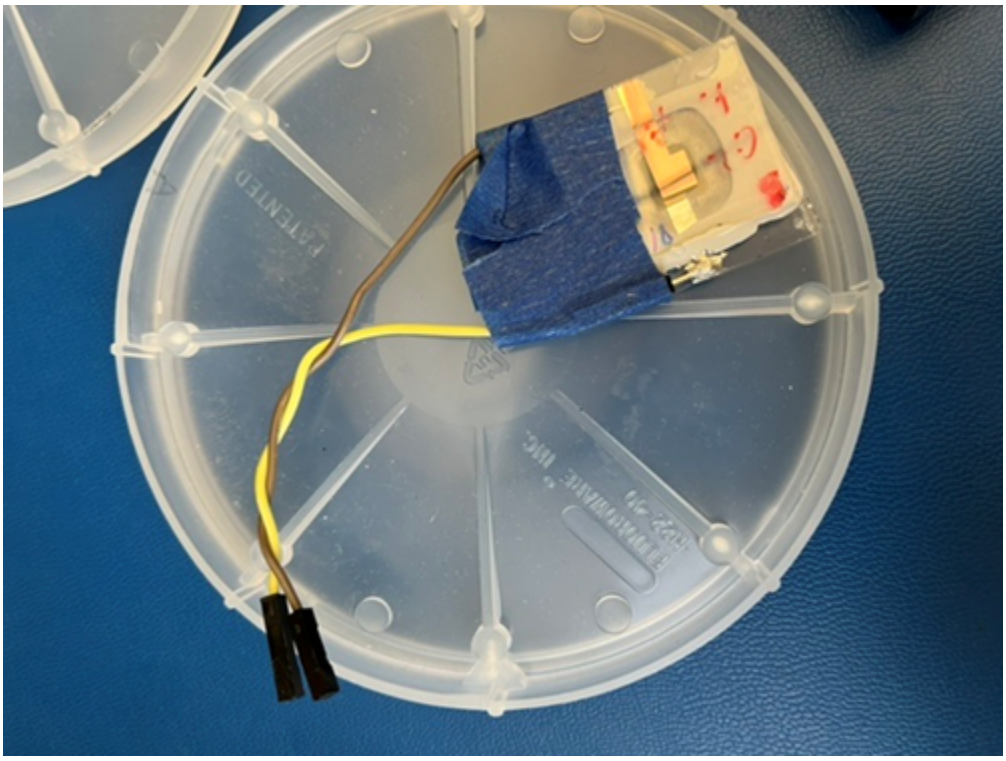

Figure 2.6: Packaged printed Lithium-ion battery [13]. Collectors are accessed via a small wire silver-epoxied to the collector contact.

2.4 OpenWSN and OpenMote

OpenWSN is an open-source IEEE 802.15.4e standards-based protocol stack for ultra low power mesh networks [6]. In order for SCμM to easily communicate over OpenWSN, an OpenMote B CC2538, as shown in figure 2.7, can be used to transmit or receive packets and send the information to a computer for analysis. The OpenMote is an open-hardware device designed to communicate and compute, designed with OpenWSN implementations in mind [9]. Furthermore, SCμM itself was designed to run OpenWSN. This makes OpenWSN an ideal method for Sulu to transmit data to an OpenMote outside the EEG-TMS-fMRI structures and for general communication in smaller fMRI or TMS only setups.

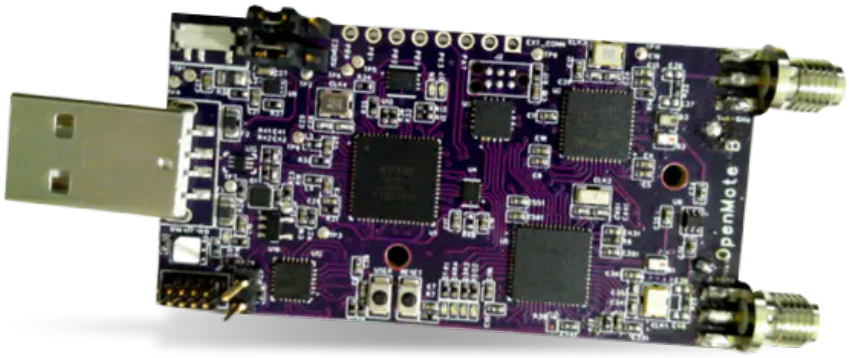

Figure 2.7: A single OpenMote B CC2538 device. For this report, an antenna was attached to one of the SMA connectors (right) while the device's USB A port (left) was plugged into a computer.

2.5 TMS, EEG, and fMRI

Electroencephalography (EEG) uses electrodes to measure the electrical field created by the billions of neurons in the cerebral cortex [12]. EEG electrodes detect microvolt level signals at low frequencies, which must be transmitted back for processing, a role Sulu provides in this project. For this project, differential measurements were chosen as the preferred method of EEG measurement, so all SCμM chips that would combine to include all electrodes in a 10-20 or 10-10 system, pictured in figure 2.8, did not require a common reference. Scalp EEG measurements are typically referred to measurements taken at an ear. However, differential measurements can greatly reduce the size of wires by connecting to two nearby electrodes instead of reaching across the head to an ear. Using a public EEG measurement dataset [20], I attempted to analyze what differential measurements, with 1-7 cm between electrodes, would look like. I selected one electrode measurement and plotted how it would appear when subtracted from EEG measurements of different electrodes 1-7 cm away. This process was then repeated with another starting electrode chosen and depicted in Figure 2.9. The goal of this test was to get a sense of how much the differential measurement would vary based on the distance between the electrodes. The data in Figure 2.9 demonstrates how smaller distances between electrodes produced similar differential measurements, but 5-7 cm between electrodes produced markedly different measurements. After further reviewing literature [5], we moved forward with the plan to use differential measurements as others have shown to repeatably be able to read electrode values differentially. When combined with other technologies such as fMRI and TMS, noticeable additional artifacts can arise in EEG measurements that must be filtered out. The microvolt level signals generated from EEG electrodes can be challenging to handle electronically and require an analog front-end to interface with SCμM. However, EEG measurements are not entirely sufficient to determine behavior inside of a brain to the best of modern tool capability and an fMRI scan can provide further detail of brain activity [5].

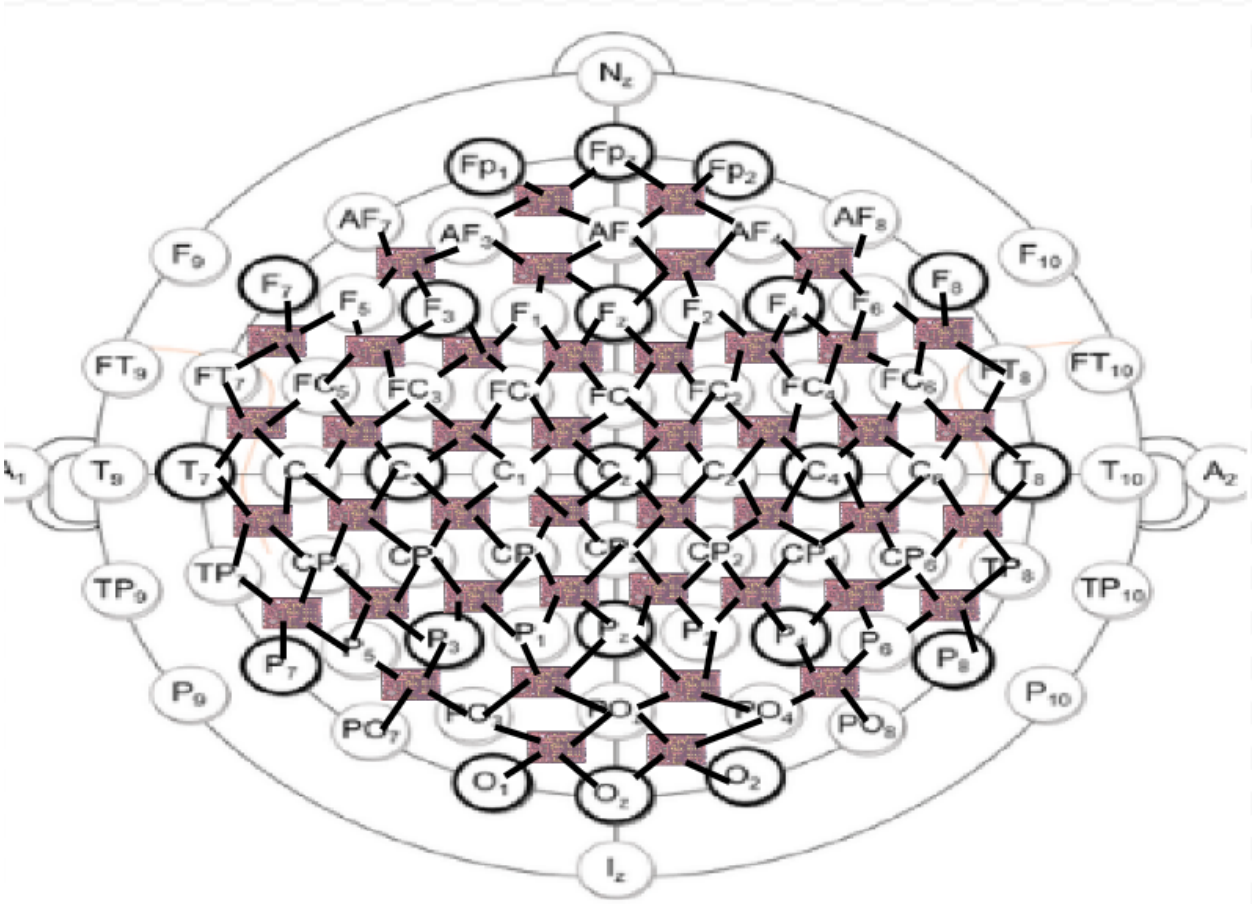

Figure 2.8: Proposed reference for SCμM location during EEG measurement. The baseline image is the standardized 10-10 electrode placement system [19]. Black lines represent which electrodes a given SCμM chip + AFE is connected to. For a given set of 4 connected electrodes, each possible subset pair of electrodes are measured differentially for a total of 6 differential pairs of measurements.

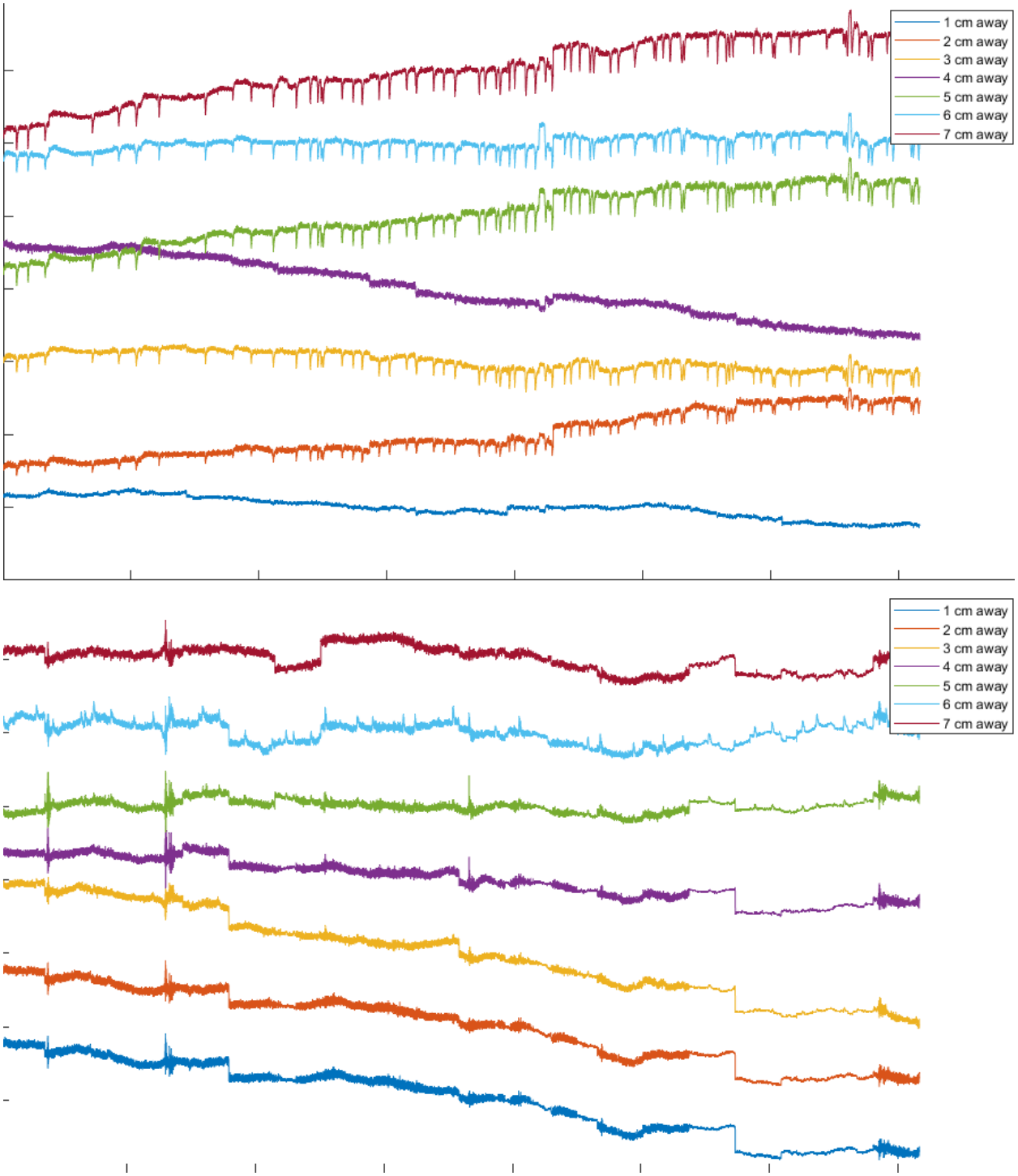

Figure 2.9: Differential measurements from an electrode relative to other electrodes 1-7 cm away from the measured electrode [20]. The two graphs represent the same test implemented two times with a different starting electrode. Differential measurements were adjusted vertically for clarity and any apparent DC offset between measurements can be ignored.

Functional Magnetic Resonance Imaging (fMRI) is a non-invasive method for measuring the activity of neurons by looking at the blood flow within a brain [14]. fMRI accomplishes this by detecting increased local cerebral blood flow and blood oxygen level dependent contrast with images captured by measuring the response of the patient in a large magnetic field [17]. A standard fMRI scan in a 3T scanner creates a linear change in the magnetic field, called a gradient, of up to 45 mT/m. This gradient helps with spatial encoding of an image. The other major component of an fMRI scan is the RF pulse. This 10-100 MHz RF pulse, also known as B1, influences the phase of the spin inside the MRI. This is represented by the direction of the change in degrees. An Echo-Planar Imaging (EPI) scan records images that take approximately 100 ms to create in rapid slices to provide a time series at each voxel. A standard EPI scan uses a roughly 25 mT/m gradient and a 90 degree (before an optional 180 degree) RF pulse. fMRI's requirement of a large magnetic field and RF pulses during a scan can initially seem incompatible with other forms of measurement such as EEG, but the two have been used in tandem with success to bolster the neuroscience information that can be interpreted [5]. Goldman et al. discuss how using dual-lead electrodes measured differentially and extensive artifact reduction post-processing on the raw EEG data can lead to an effective combined EEG and fMRI analysis of brain-behavior.

Transcranial Magnetic Stimulation (TMS) is a way to stimulate brain activity using the movement of a coil noninvasively that moves around the edge of a patient's head, delivering magnetic pulses like those in figure 2.10. TMS applies a pulse typically over hundreds of microseconds to a region in someone's head via a large pulse that can use current on a kiloamp scale and supply a voltage up to roughly 10 kV [15]. The exact parameters of the TMS pulse are typically given with the amplitude of the pulse as a percentage of the TMS machine's maximum output. TMS pulses for this project are typically biphasic, with a large negative pulse followed by a large positive oneness represented in Figure 2.10. To reduce the impact of the sound of TMS pulses, quiet TMS has been discussed to change the frequency above the human hearing range and a corresponding increase in

current and voltage pulse amplitude [16]. An everyday use for TMS is as a treatment for depression where a train of repetitive TMS pulses can be applied to a patient's prefrontal cortex[15].

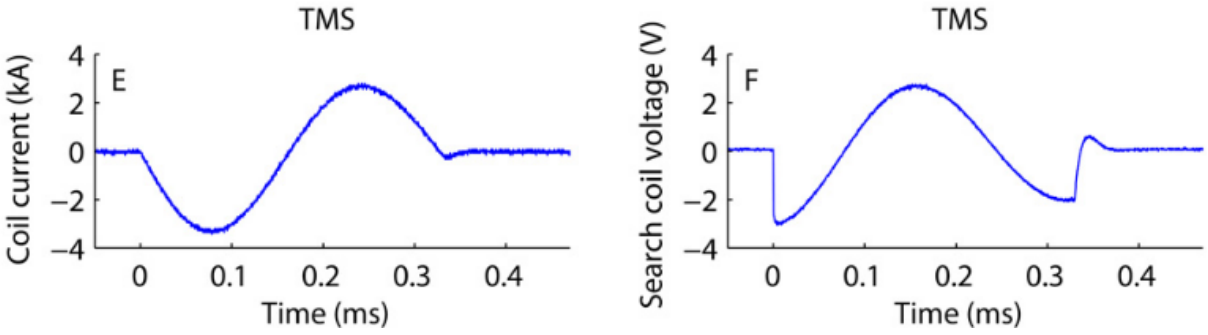

Figure 2.10: Sample transcranial electromagnetic stimulation waveforms [15]. A Magstim Rapid generated the TMS pulse set to 67% of the device maximum. The current in the TMS coil was recorded (left). A 1 cm x 30 cm search coil was positioned perpendicular to the TMS coil plane with a measured voltage (right) proportional to the voltage in the TMS coil.

Conde et al. [11] describe how TMS aftereffects can be accurately measured by evaluating EEG activity around the site TMS was applied. Thut et al. [10] further demonstrate how EEG electrodes can pick up a robust 30-35% change on average from a baseline measurement for up to an hour after TMS usage. Given the much shorter TMS pulse length of hundreds of microseconds, the worst case electromotive force generated by the TMS pulse will be at least 3 orders of magnitude higher than the electromotive force generated by an MRI scan. The voltage induced by a TMS coil can be calculated using $\epsilon = \frac{d\phi}{dt} = A\frac{dB}{dt}$ by Lenz's law. The coil available at the Berkeley Brain Imaging Center, the Cool-B65, has a maximum $\frac{dB}{dt} = 36\ kT/s$ for $\epsilon = 3.6V$ for a $1\ cm^2$ loop. As such, any loops need to be as small as possible when considering board design.

Chapter 3

Testing SCμM in EEG, TMS, and fMRI Environments

3.1 Sulu Transmitting EEG Signals

In this project, Sulu needs to be able to detect the microvolt EEG signals from electrodes connected to the scalp of a patient and transmit their data wirelessly to a nearby receiver for further evaluation and to determine the following TMS treatment location and intensity. The signal must be transmitted wirelessly as extensive wired connections would cause a spatial conflict with the TMS coil robot and otherwise attaching long cables to a patient during these treatments represents an unnecessary additional health risk. As such, SCμM will use its 2.4 GHz radio to transmit the necessary data during the desired scan period.

The ADC built into SCμM is not designed to be directly compatible with signals at such a low voltage input to the chip, nor was it designed to interface specifically with EEG signals in a noisy environment. As a result, the ADS1299 was chosen to provide an EEG analog front end for a board-level solution to the problem. The ADS1299 operates at 1.8V on digital I/O which is compatible with Sulu and communicates via the standardized Serial Peripheral Interface (SPI) that has been well-established to interact well with SCμM on Sulu boards.

Additionally, it can take in differential measurements similar to those desired for the larger project instead of measurements that share a common reference. The ADS1299 can be programmed to select which electrode inputs it desires to read from and feeds their data through a low-noise programmable gain amplifier and a 24-bit ADC to convert them to

digital information with the same 1.8V reference as SCμM. When Chekov indicates that it is ready for the information to be received, the ADS1299 transmits up to 216 bits of data containing the measured voltages after receiving the DREADY command over SPI.

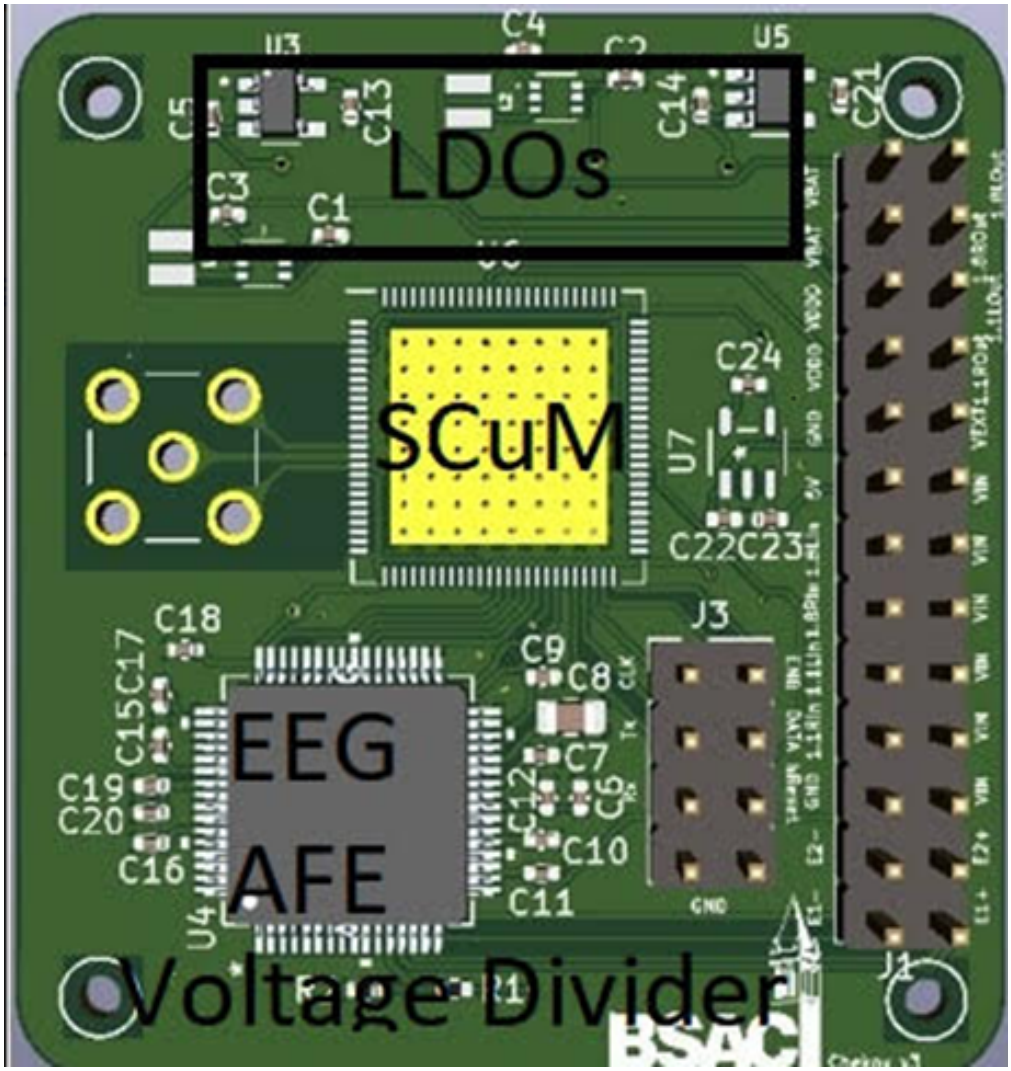

Figure 3.1: 3D markup of SCμM Chekov v3 development board. Pictured are LDOs and possible DC-DC Converter alternative footprints (upper quarter), ADS 1299-4 EEG Analog Front End (bottom left), test voltage divider (below ADS 1299-4), power connections (left 2 rows of pin headers), and external communication connections (central 2 rows of pin headers). A link to the board design can be found in Appendix B.

A SCμM development board named Chekov, pictured in figure 3.1, was designed to accommodate the interaction between SCμM and the ADS1299. This board was created in order to test Chekov with microvolt level signals in an MRI without having to run cables before a custom EEG ADC and amplifier can be developed. The 4-channel version of the ADS1299, the ADS1299-4, was deemed sufficient for tests verifying functionality with SCμM. The DC-DC converters found on the Sulu development boards and an LDO alternative were supplied. Two options were included in anticipation of ongoing electronic component shortages. Which option is used can be selected by placing jumpers in distinct locations on the pin headers on the left side of the board. UART and 3WB connections were also added to the right of the power connections closer to SCμM, although a boot source select signal must be applied separately to SCμM to take full advantage of its 3WB programming.

A SCμM GPIO pin is tied to a voltage divider located immediately below the ADS1299-4 as seen in Figure 3.1. This was included to generate a 5 microvolt level test signal fed directly into an ADS1299-4 electrode input if that GPIO pin on SCμM is held high at 1.8V. A five microvolt signal was chosen because it is comparable to typical EEG measurements. This voltage divider did not have the option to be disconnected from SCμM on the Chekov v3 design. The lack of isolation between the voltage divider and SCμM potentially damaged the SCμM chip when Chekov was powered as described below.

After assembly, an issue arose with the functionality of the packaged SCμM chips on the PCB. The current drawn by the combined input to the packaged SCμM chip and the ADS1299-4 was 3 mA higher than expected. During attempts to program the SCμM on the Chekov development boards, connection to the SCμM chip itself was verified as it maintained a characteristic current jump. However, the unprogrammed current drawn was around 3.7 mA, about 3.4 mA higher than expected based on testing with other SCμM chips and the packaged SCμM chips on Chekov when they were tested before assembly. Given this result held after removing the

ADS1299-4 and voltage divider, it is likely that one of those connections damaged the connected SCμM on the initial testing attempts.

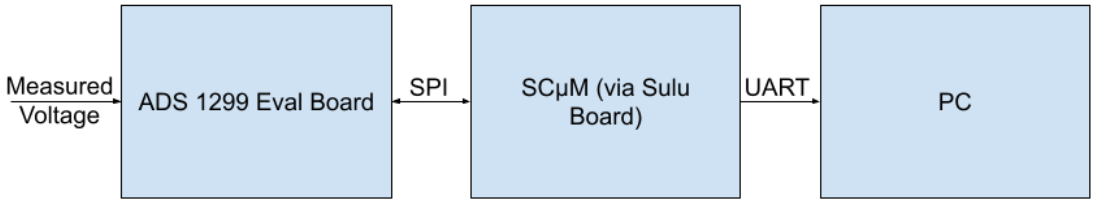

Figure 3.2: Connections between Sulu, an ADS 1299-4 eval board, and a PC. A voltage is applied across electrode measurement pins for the ADS1299-4. The reading from the ADC in the ADS-1299-4 is then transmitted to Sulu via SPI. Sulu then prints the information it receives over UART to be read by a serial monitor on a PC.

In a separate test, Sulu was able to communicate with an off-chip ADS1299 evaluation board powered separately as described in Figure 3.2. To verify the performance of the ADS1299, mV pulse at 1 kHz was applied to an RC circuit with a 1 ms time constant to create a decaying pulse as shown in Figure 3.3. The results, in Figure 3.4, showed the ability for the ADS1299 to recreate the 3dB decay expected for the test circuit in Figure 3.3.

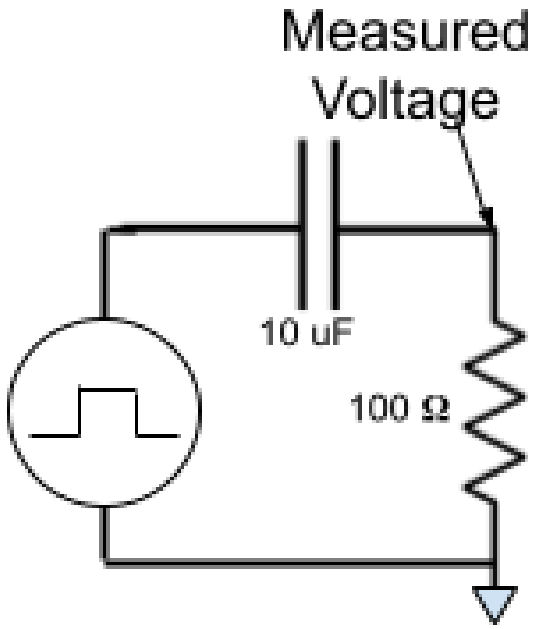

Figure 3.3: Test circuit for ADS1299 eval board communication test. The point between the resistor and capacitor was measured by both an oscilloscope and connected to the ADS1299 eval board.

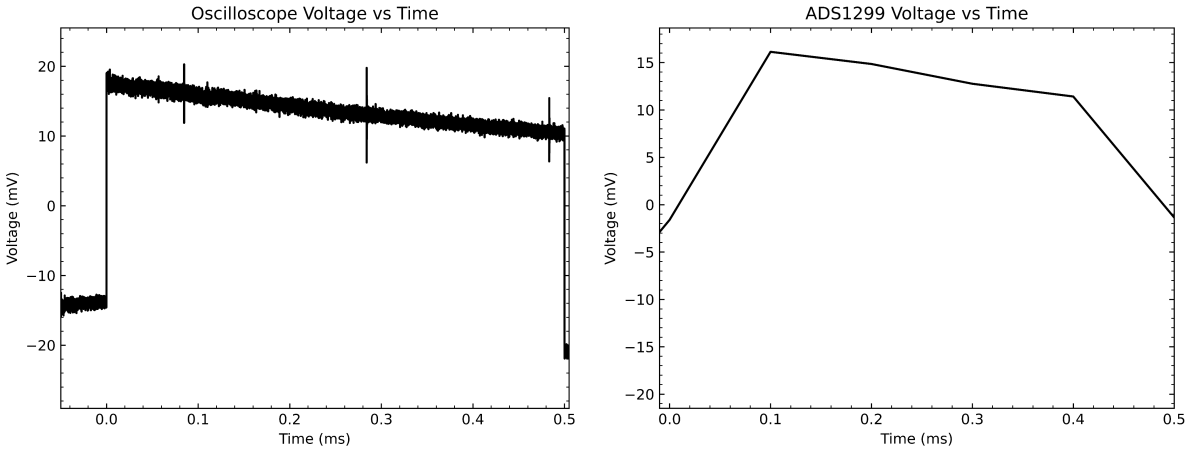

Figure 3.4: Measured output of test circuit in Figure 3.3 from an oscilloscope (left) and ADS1299 eval board (right).

3.2 SCμM Transmitting during an MRI

In order for SCμM to be involved in this project, it was necessary to confirm its compatibility to perform packet transmission inside an MRI environment similar to one that would occur during a full implementation of the larger TMS-EEG-fMRI project. Once it was confirmed that Sulu and the printed lithium-ion batteries were non-magnetic and therefore safe to incorporate into a design, their individual functionality during scanning needed to be tested. Sulu was first tested with a known MRI-safe battery and then verified with a printed lithium-ion battery to isolate any potential issues.

Initially, a GM-NM103450 MRI safe battery was chosen for the test duration. SCμM was programmed with firmware, provided in Appendix C, that swept a narrow range of frequencies established to provide a strong connection between the individual SCμM chip used and the OpenMote that would be incorporated in the test. Once the firmware was programmed onto SCμM, the nRF52840-DK was disconnected, and Sulu was placed inside the scanner's bore. Meanwhile, an antenna connected to an OpenMote attached to a computer for data recording was fed through the conduit between the operator room and magnet room. A 2.3 GHz high pass filter was inserted between the antenna and OpenMote to reject RF energy from a scan coupled to the line. The overall setup is described in figure 3.5.

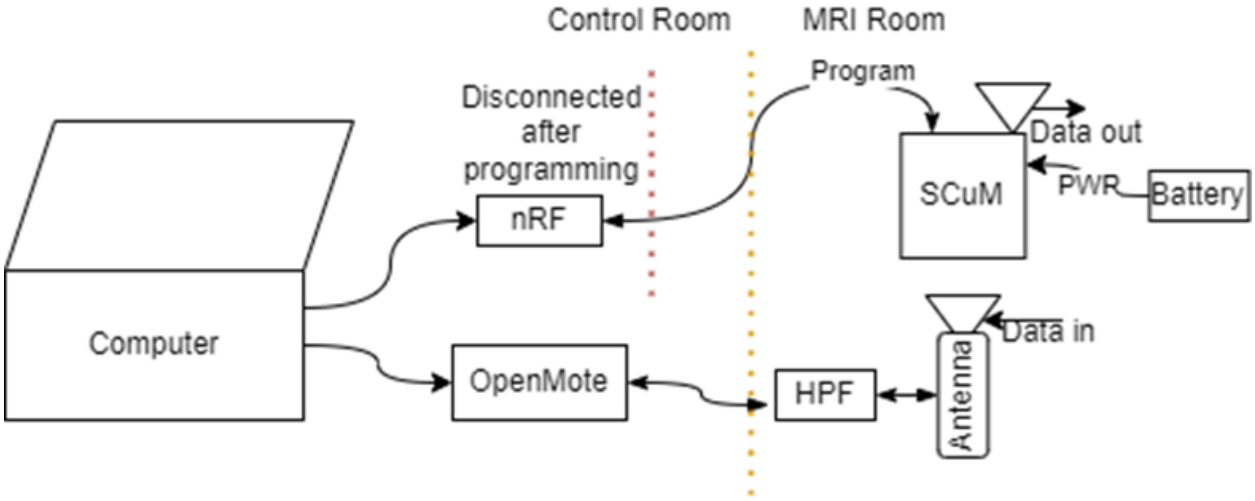

Figure 3.5: Diagram of SCμM connections during MRI tests. A SCμM Sulu development board connected to an MRI-safe battery is placed inside the scanner during the scan, with the antenna also in the scanner room sending the data it picks up back to a computer for analysis via an OpenMote.

Sulu was tested in this configuration with scans of increasing length and RF, gradient, or both components. First, a simple gradient scan with no RF pulse, a simple RF scan with no gradient, and the combined scan with both gradient and RF pulses were administered to verify functionality. Next, a localizer body scan and a B1 map body scan were run in order to confirm that Sulu continued to transmit data during common body scans as well. Finally, most of the evaluation of Sulu's performance under an MRI scan was performed with the EPI scan described in section 2.5. When testing with the known MRI-safe battery, it could be seen that there was no noticeable change in performance during a scan with gradient and no RF pulses. A sample of the output seen from the OpenMote is pictured in Figure 3.6. However, there was a drop of roughly 2 RSSI and about 1% worse byte error rate when using scans with RF. No consistent change in dropped packet rate could be found for any scan. Likewise, the only distinguishable change when moving Sulu from the center of the scanner's bed, as in figure 3.8, to the bore, as in figure 3.7, was a drop in RSSI from roughly -75 to -90 dBm and an increase in the byte error rate of roughly 4%. In an attempt to increase the RSSI, the test with the EPI scan was

repeated with the receiver antenna placed in the MRI bore just above where Sulu is pictured in Figure 3.7. Interestingly, there was no noticeable difference in RSSI, missing packet rate, or byte error rate if the antenna was also placed in the bore or simply through the conduit described above.

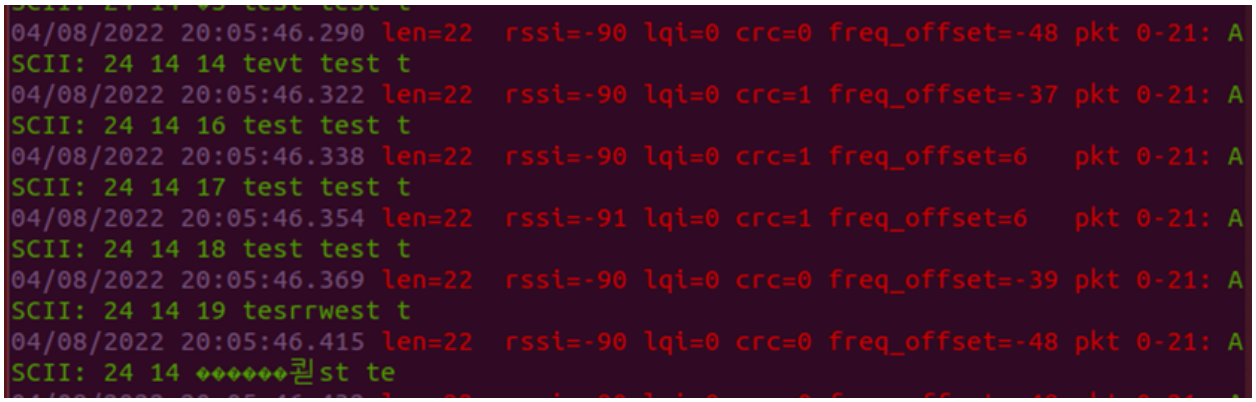

Figure 3.6: Sample terminal output for SCμM Sulu development board transmitting to a single OpenMote B CC2538 device. In this scenario, SCμM is programmed to transmit a length 20 packet with 2 CRC bytes containing the coarse, medium, and fine SCμM frequency values and the word “test” to fill up the rest of the length 20 packet body. Various parameters regarding packet transmission are recorded and printed to the terminal and an output log for evaluation. The first and last two packets listed in this sample output have byte errors.

SCμM location	Average RSSI [dBm]	Missing Packet Rate	Byte Error Rate
Operator Room	-35	0%	0%
Bed of scanner with GM-NM103450	Before scan: -75 During scan: -77	Before scan: 2% During scan: 2%	Before scan: 4% During scan: 6%
Scanner bore with GM-NM103450	Before scan: -89 During scan: -91	Before scan: 3% During scan: 2%	Before scan: 8% During scan: 9%
Bed of scanner with printed battery	Before scan: -70 During scan: -71	Before scan: 0% During scan: 0%	Before scan: 3% During scan: 4%
Scanner bore with printed battery	Before scan: -80 During scan: -85	Before scan: 4% During scan: 4%	Before scan: 9% During scan: 10%

Table 3.1: Results from testing Sulu transmission performance consistent under all MRI scans with RF pulses. Statistics were recorded before a scan started and while the scan was implemented. Performance was also measured prior to placing any component in the scanner room to get a picture of ideal results. Over 100 packets were sent for each test represented in this table.

Sulu was then powered by a printed lithium-ion battery attached via 8331-D silver conductive epoxy. A printed battery-powered Sulu is able to clearly transmit information during EPI scans emblematic of scans utilized by the larger TMS-EEG-fMRI project. The results were similar to those described with the GM-NM103450 battery. As such, there is reason to believe similar performance can be achieved on smaller scale Sulu + printed battery designs that sit near a patient's scalp.

Figure 3.7: Image of SCμM Sulu development board in the bore of a 3T MRI machine immediately prior to testing performance during a performance test.

Figure 3.8: Close-up of semi-open structure SCμM Sulu development board was placed within with MRI coils designed by Julian Maravilla intended to be used in combined TMS-EEG-fMRI project. The total overall structure was tested both in the bore as pictured in figure 3.7 and on the bed of the scanner pictured here (left). Openmote B with antenna and high pass filter in the corner of the scanner room connected through the conduit into operator room (right).

3.3 SCμM Functionality after TMS Pulses

It needs to be shown that SCμM is also resistant to a nearby TMS pulse of various amplitudes and settings. This is important as it is desired that a robot-controlled TMS coil is able to freely move around a patient's head and administer treatment as deemed necessary. Sulu was first tested with low amplitude signals. The signal amplitude was then slowly ramped up in order to isolate any potential issues.

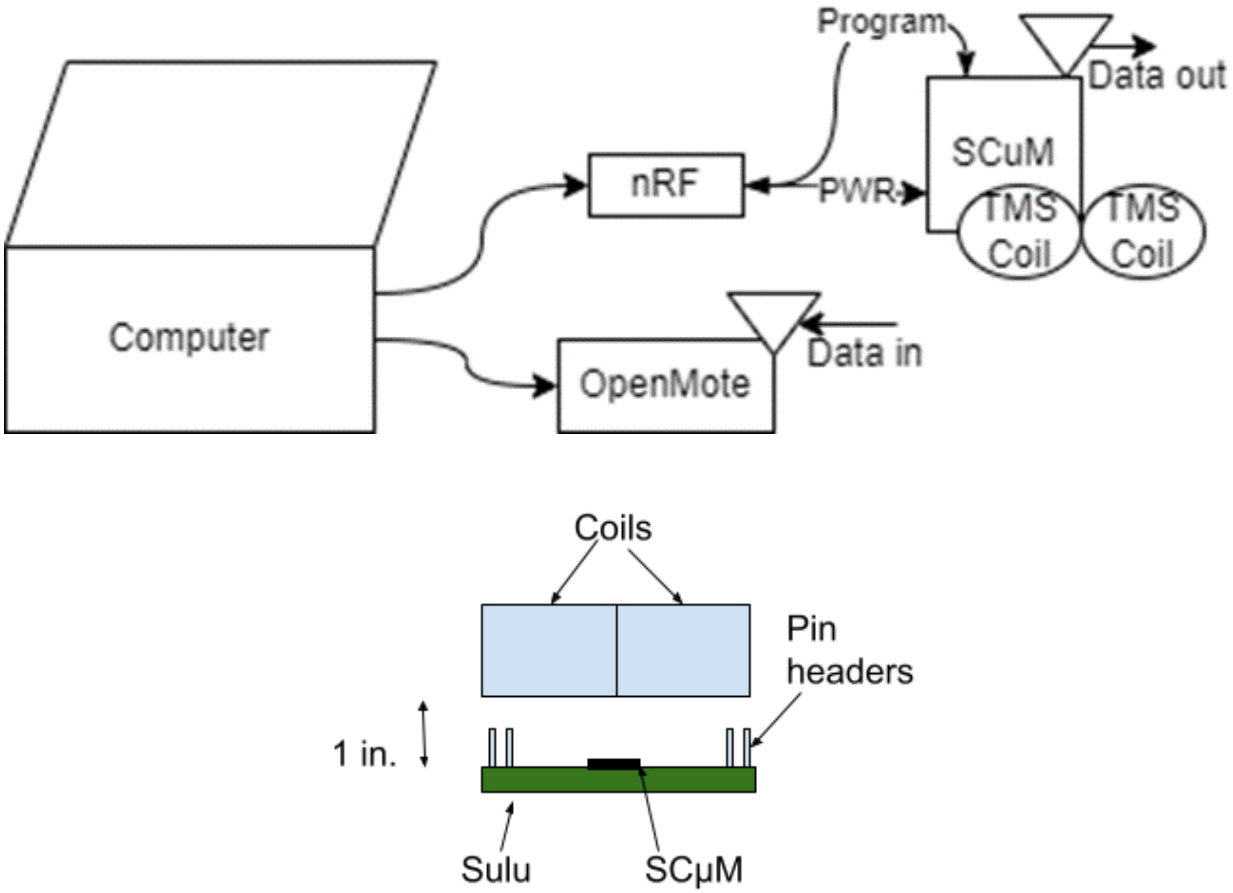

Figure 3.9: Diagram of initial Sulu connections during TMS tests. A SCμM Sulu development board, connected to the nRF52840-DK as a 5V power source, is placed roughly an inch below the center of a TMS coil during the test with the nearby OpenMote sending transmission data back to a computer for analysis. An overall diagram is pictured (top) as well as a side-view (bottom) of the TMS coils and Sulu.

To verify the functionality of Sulu after a TMS pulse, a setup similar to that found in the previously detailed MRI test of Sulu's durability was assembled, as detailed in Figure 3.9. The coil was placed approximately 1 inch above the SCμM chip on Sulu for all tests with the SCμM chip centered on the center of the figure 8 coil structure between the two coils. Initially, the nRF52840-DK was connected such that it acted both as a programmer for the Sulu development board and as a 5V power supply. Sulu's behavior patterns under different amplitudes was characterized by testing over a wide range of options. The testing procedure initially

confirmed functionality at very low amplitude percentages, verifying 1, 2, and 3% were satisfactory before increasing in steps of 10%. The test continued until Sulu died and needed to be reset. After reset, the amplitude would be fine-tuned until the exact amplitude generating failure was found. The same frequency sweep program found in Appendix C would be used that rotated through the best frequency settings for communication found between the specific Sulu board and OpenMote at first. When Sulu first appeared to die, a much wider range frequency sweep program was tested to determine if the ideal operating frequency setting had simply been altered or if Sulu did die and need to be reset. Similarly, a train of 3 TMS pulses in quick succession would be tested around the amplitude where a change in behavior was first noticed in order to detect if the details would be altered by more than one biphasic pulse's involvement. The amplitude generating failure held constant as the firmware frequency sweep range and number of TMS pulses in a train increased.

Figure 3.10: MagPro X100 TMS machine and Cool-B65 coil used for TMS tests (top). Example of settings of TMS MagPro X100 machine during the TMS test (bottom). Single biphasic pulses initiated manually on the coil made up the recent tests were administered before this photo was taken, as demonstrated by the upper right of the display.

For this iteration of the test, no alteration in packet error rate was found for any pulses delivered while the relative amplitude was below 47%. For this range of TMS pulses, Sulu behaved indistinguishably from how it was acting before the test. A sample of the TMS settings for this test can be seen in Figure 3.10. However, for all tested amplitudes of 48% or higher, packet reception by the OpenMote abruptly stopped. This signified Sulu needed to be reprogrammed. However, no power cycle was necessary to restart packet transmission.

The same testing configuration using LDOs to step down the 5V input instead of the DC-DC converter alternative was evaluated, but no change was registered. In an attempt to isolate the issue, a separate battery was used to power the Sulu development board as demonstrated in Figure 3.11 and all connections to the nRF52840 were disconnected after programming.

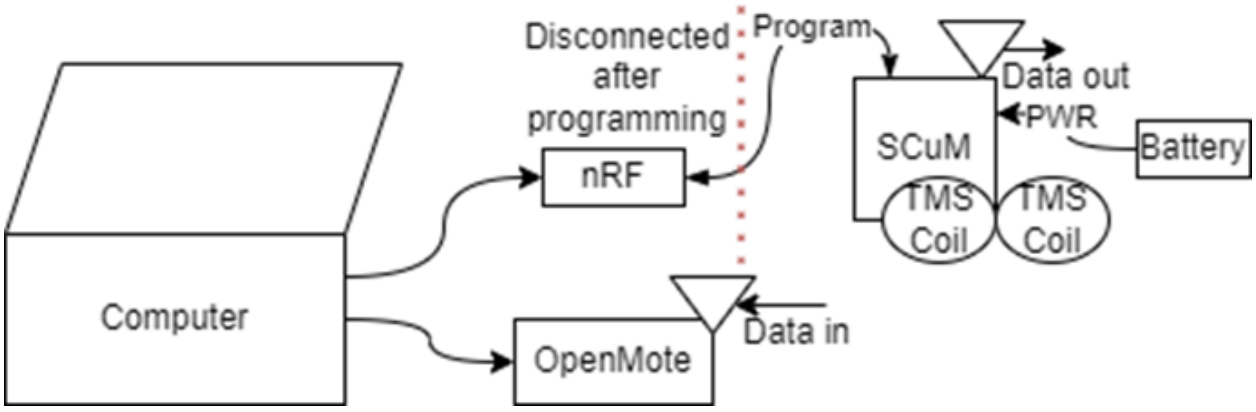

Figure 3.11: Diagram of revised Sulu connections during TMS tests. A SCμM Sulu development board connected to a battery is placed roughly an inch below the center of a TMS coil during the test with the nearby OpenMote sending transmission data back to a computer for analysis.

This modified setup generated significantly more promising results outlined in Table 3.2. At this point, the cutoff relative amplitude where the OpenMote

stopped receiving packets was at 97% maximum amplitude. Once again, this result held under wider frequency sweep ranges and TMS pulse train lengths indicating something in the large amplitude pulses caused SCμM to essentially reset its programming. The same Sulu development board was used for all tests and for many unrelated SCμM functions with no recognizable long-term effects in behavior. This observed operation indicates that Sulu should not have any issues transmitting packets as long as a nearby TMS pulse is below a certain amplitude threshold.

Amplitude	Average RSSI	Missing Packet Rate	Byte Error Rate
Before Test	-48	0%	0%
1%	-48	0%	0%
2%	-48	0%	0%
3%	-48	0%	0%
10%	-47	0%	0%
20%	-47	2%	1%
30%	-47	0%	0%
40%	-46	0%	0%
50%	-46	2%	0%
60%	-47	0%	1%
70%	-47	0%	0%
80%	-48	0%	0%
90%	-48	0%	0%
95%	-47	0%	0%
96%	-50	0%	3%
97%	-48	0%	0%
98%	N/A	100%	N/A
99%	N/A	100%	N/A

Table 3.2: Results of single biphasic TMS pulses applied with the center of the TMS coil approximately an inch above the SCμM chip on Sulu as the output amplitude was varied across the range of the MagPro 100X's output amplitude capabilities.

Chapter 4

Conclusion

This report details SCμM's capability in withstanding TMS and fMRI environments to transmit EEG data for prompt analysis in a connected operator room. The proposed idea of SCμM's role within that larger TMS-EEG-fMRI project should be feasible with no measurable harm to SCμM's functionality. Standard MRI scans such as EPI scans and biphasic TMS pulses as expected to be integrated, would not be expected to disrupt SCμM's operation. Likewise, SCμM's ability to interface with SPI devices and send that information wirelessly will allow an ADS1299 or other EEG analog front-end to convert electrode readings to a measurement that SCμM can understand. With the number of potential SCμM applications ever-expanding, durability in specialized testing environments can drastically increase the effectiveness of modern medical treatments that rely on SCμM for basic functionality. However, solutions could vastly still be improved upon as the final design for an integrated TMS-EEG-fMRI system is designed as described below.

The Chekov development board could be further optimized based on the tested results and shrunk to a design close to the 2x3x0.3 mm^3 the SCμM chip itself is that involves a directly wire-bonded SCμM without the extra package space and no excess pins, voltage converters, or other components. The presented Chekov v3 board is not necessarily the ideal final result for integrating SCμM into a more extensive system outlined in the TMS-EEG-fMRI project. That is a role better fit for a custom chip either to be paired with SCμM or to incorporate as a part of a new version of SCμM and implemented directly next to an electrode grouping.

It is also possible that the TMS survivability measurements did not manage to capture a worst-case scenario. Further testing can place the SCμM chip on Sulu perpendicular to the TMS coil instead of parallel to it or have the

SCμM chip on Sulu centered on one of the loops of the TMS coil instead of on the center of it. Once there is more clarity on what fMRI scans precisely will be used, attempts to intersperse those scans with TMS pulses can confirm SCμM's behavior in a realistic testing environment. Similar system integration level testing will be needed before the proposed setup is ready for widespread use.

In general, SCμM and any related components necessary for EEG recording and transmission will eventually be attached to a cap for a patient to wear. A typical configuration for EEG electrode placement will need to accommodate for SCμM chips to have up to 64 channels accessed at once. Considerations with custom MRI coils will also have to be fully taken into account. The variations in location for each of the SCμM chips in this design will allow for some to have more obstructions that could block Sulu transmission signals while others would be more out in the open. Adding components to handle blocking signals on the transmission side, in addition to the high pass filter on the receiving end of the signal, can also possibly improve signal strength and error rate.

Overall, Sulu was shown to transmit packets from inside the bore of an MRI during a scan using both a commercial MRI-safe battery and a custom printed battery. Sulu was shown to withstand TMS pulses of 47% of a MagPro X100's power when connected to an nRF52840-DK. That amplitude increased to 97% when Sulu was instead connected to a commercial battery. Finally, Sulu was shown to interface with an ADS1299 development board over SPI and transmit packets to an OpenMote receiver.

Bibliography:

[1] F. Maksimovic et al., "A Crystal-Free Single-Chip Micro Mote with Integrated 802.15.4 Compatible Transceiver, sub-mW BLE Compatible Beacon Transmitter, and Cortex M0," 2019 Symposium on VLSI Circuits, 2019, pp. C88-C89, doi: 10.23919/VLSIC.2019.8777971.

[2] Moreno, Alex et al. “Single-Chip micro-Mote for Microrobotic Platforms.” (2020).

[3] Moreno, Alexis. “Small Autonomous Robot Actuator (SARA): A Solar-powered Wireless MEMS Gripper”. EECS Department, University of California, Berkeley, 2021.

[4] Yau, Jeffrey M et al. “Static field influences on transcranial magnetic stimulation: considerations for TMS in the scanner environment.” Brain stimulation vol. 7,3 (2014): 388-93. doi:10.1016/j.brs.2014.02.007

[5] Goldman, R I et al. “Acquiring simultaneous EEG and functional MRI.” Clinical neurophysiology : official journal of the International Federation of Clinical Neurophysiology vol. 111,11 (2000): 1974-80. doi:10.1016/s1388-2457(00)00456-9

[6] Watteyne, T., Vilajosana, X., Kerkez, B., Chraim, F., Weekly, K., Wang, Q., Glaser, S. and Pister, K. (2012), OpenWSN: a standards-based low-power wireless development environment. Trans. Emerging Tel. Tech., 23: 480-493. https://doi.org/10.1002/ett.2558

[7] Burnett, David. “Crystal-free wireless communication with relaxation oscillators and its applications”. EECS Department, University of California, Berkeley, 2019.

[8] T. Watteyne, "Crystal-Free Architectures for Smart Dust and the Industrial IoT," 2020 7th International Conference on Internet of Things: Systems, Management and Security (IOTSMS), 2020, pp. 1-1, doi: 10.1109/IOTSMS52051.2020.9340195.

[9] Xavier Vilajosana et al. “OpenMote: Open-Source Prototyping Platform for the Industrial IoT”. In: International Conference on Ad Hoc Networks (AdHocNets). San Remo, Italy, Sept. 2015, pp. 211–222. doi: 10.1007/978-3-319-25067-0_17.

[10] Thut, Gregor, and Alvaro Pascual-Leone. “A review of combined TMS-EEG studies to characterize lasting effects of repetitive TMS and assess their usefulness in cognitive and clinical neuroscience.” Brain topography vol. 22,4 (2010): 219-32. doi:10.1007/s10548-009-0115-4
[11] Conde, Virginia et al. “The non-transcranial TMS-evoked potential is an inherent source of ambiguity in TMS-EEG studies.” NeuroImage vol. 185 (2019): 300-312. doi:10.1016/j.neuroimage.2018.10.052
[12] R. B. Paranjape, J. Mahovsky, L. Benedicenti and Z. Koles', "The electroencephalogram as a biometric," Canadian Conference on Electrical and Computer Engineering 2001. Conference Proceedings (Cat. No.01TH8555), 2001, pp. 1363-1366 vol.2, doi: 10.1109/CCECE.2001.933649.
[13] Toor, Anju et al. “Stencil-printed Lithium-ion micro batteries for IoT applications”. Nano Energy 82 (2021): 105666.
[14] Heeger, D., Ress, D. What does fMRI tell us about neuronal activity?. Nat Rev Neurosci 3, 142–151 (2002). https://doi.org/10.1038/nrn730
[15] Peterchev, Angel V et al. “Fundamentals of transcranial electric and magnetic stimulation dose: definition, selection, and reporting practices.” Brain stimulation vol. 5,4 (2012): 435-53. doi:10.1016/j.brs.2011.10.001
[16] Peterchev, Angel V et al. “Quiet transcranial magnetic stimulation: Status and future directions.” Annual International Conference of the IEEE Engineering in Medicine and Biology Society. IEEE Engineering in Medicine and Biology Society. Annual International Conference vol. 2015 (2015): 226-9. doi:10.1109/EMBC.2015.7318341
[17] Glover, Gary H. “Overview of functional magnetic resonance imaging.” Neurosurgery clinics of North America vol. 22,2 (2011): 133-9, vii. doi:10.1016/j.nec.2010.11.001
[18] Kilberg, Brian. ‘Actuation and Localization of Resource-Constrained Autonomous Microrobotic Systems’. EECS Department, University of California, Berkeley, 2021.
[19] Hong, Seunghyeok & Baek, Hyun. (2021). Drowsiness Detection Based on Intelligent Systems with Nonlinear Features for Optimal Placement of Encephalogram Electrodes on the Cerebral Area. Sensors. 21. 1255. 10.3390/s21041255.

[20] Cho, H., M. Ahn, and S. Ahn. "Supporting data for “EEG datasets for motor imagery brain computer interface.”." GigaScience Database (2017).

Appendix A

Packet Evaluation script

A python script for evaluating reception parameters of packets printed to a log file can be found at:

https://github.com/joshalexander1315/SCuM-packet-params

Appendix B

Chekov Development Board Design Files

KiCAD files for the Chekov v3 development board can be found at https://github.com/PisterLab/scum-dev-board/tree/eeg-mri/chekov

Appendix C

Sulu Frequency Sweep Code

C code for programming Sulu to sweep over a small range of frequencies can be found at https://github.com/PisterLab/scum-test-code/tree/develop/scm_v3c/applications/freq_sweep_tx

Appendix D

Sulu ADS1299-4 Communication Code

C code for programming Sulu to interact with the ADS1299-4 EEG AFE can be found at https://github.com/joshalexander1315/scum-test-code/tree/develop/scm_v3c/applications/log_AFE